Available online at www.sciencedirect.com
SCIENCE DIRECT
Journal of Colloid and Interface Science 285 (2005) 581–589
JOURNAL OF Colloid and Interface Science
www.elsevier.com/locate/jcis

Contamination by larger particles of two almost-uniform latices: analysis by combined dynamic light scattering and turbidimetry

Verónica D.G. Gonzalez, Luis M. Gugliotta, Jorge R. Vega, Gregorio R. Meira *

INTEC (Universidad Nacional del Litoral and CONICET), Güemes 3450, (3000) Santa Fe, Argentina

Received 29 December 2003; accepted 2 December 2004

Available online 5 February 2005

Abstract

Multiangle dynamic light scattering (MDLS) and turbidimetry (T) were applied (both individually and combined) for determining the contamination by larger particles of two almost-uniform polystyrene (PS) latices. Latex 1 was synthesized in our laboratories, and it contained a main population diameter of 340 nm together with a small fraction of larger particles. This latex was used as the base material for producing an immunoassay kit. Latex 2 was obtained by a simple blend of two uniform PS standards. The proposed data treatment calculates the diameter and number fraction of the large particles contamination assuming that the PSDs are bimodal. The calculation involves minimizing the errors between the measurements and their theoretical predictions. When analyzed by combined MDLS–T, the contamination of Latex 1 involved number fraction 0.6% and particle diameter 865 nm. The T average diameter is a function of the measurement wavelength, and the highest deviations of this average to an increasing contamination by large particles were always observed at the higher wavelengths. The DLS average diameter is a function of the measurement angle, but in this case it is impossible to determine a priori the angle of observation that provides the largest deviation of this average diameter to an increasing contamination.

Keywords: Multiangle DLS; Turbidimetry; Monodisperse latex

1. Introduction

A set of particles is uniform or monodisperse when all the particles exhibit a common size and shape. Uniform particles find application in catalysts, ceramics, electromagnetic materials, photographic emulsions, pigments, etc. In particular, uniform and spherical polystyrene (PS) latices are used as calibration standards in electron microscopy and as solid supports in medicine and pharmacy [1,2]. Uniform latices are produced by dispersion or emulsion polymerizations. In both of these processes, the reaction temperature and stirring rate must be adequately controlled, the nucleation stage must be short, the particle growth must be approximately constant, and the following must be avoided: multiple nucleation, random coagulation, and the presence of impurities or inhibitors [1,3].

In this work, multiangle dynamic light scattering (MDLS), turbidimetry (T), and scanning electron microscopy (SEM) were applied to determine the contamination of two similar PS latices by large particles. Latex 1 was synthesized in our laboratories through emulsifier-free emulsion polymerization, and its characterization motivated the present work. Latex 1 was used as the base material for developing an immunoassay agglutination test kit aimed at detecting the Chagas disease [4]. Latex 2 was similar to Latex 1, but it was "artificially" produced by simple blend of two uniform PS standards. In Latex 2, a bimodal particle size distribution (PSD) was sought, as is required by the proposed data treatment.

Immunoassay latices are normally uniform for (a) increasing their colloidal stability; (b) more easily calculating the total particle area; (c) obtaining a homogeneous distribution of the diagnosis protein onto the particles surface;

* Corresponding author. Fax: +54-342-455-0944.
E-mail address: gmeira@ceride.gov.ar (G.R. Meira).

0021-9797/$ – see front matter
doi:10.1016/j.jcis.2004.12.001

and (d) more easily visualizing the agglutination process. To produce the immunoassay kit, Latex 1 was first functionalized with carboxyl groups, and then a recombinant antigen of *Trypanosoma cruzi* was covalently coupled onto the carboxyl groups, to produce the final protein–latex complex [2]. The carboxylation of Latex 1 was carried out through a copolymerization of styrene and methacrylic acid, with Latex 1 used as seed. The resulting hydrophilic shell increased the stability of the base latex.

In conventional emulsion polymerizations with soap, most polymer particles are generated from the initial soap micelles. In this case, the polymer particles generated from the monomer droplets are negligible in number, because their surface area is several orders of magnitude lower than the surface area of the soap micelles. In contrast, in a soap-free emulsion polymerization, the main particle-formation mechanism is the so-called homogeneous nucleation. In this case, the final PSD is expected to contain a (smaller-sized and almost-uniform) main population generated by homogeneous nucleation, together with a small fraction of larger particles originated by polymerization in the monomer droplets [3,4].

Transmission and scanning electron microscopy (TEM and SEM, respectively) are the main reference techniques for observing and characterizing latices. The disadvantages of electron microscopy are, however, that (a) the measurements are expensive and time-consuming; (b) the sample preparation is complex (the particles must be isolated from the dispersion medium, special treatments are necessary to avoid particle distortion, and a gold coverage may be required to avoid particle damage by the electron beam); and (c) the PSD evaluation may involve measuring and counting thousands of particles [5,6].

The investigated optical techniques (MDLS and T) provide fast and reasonably good estimates of the average particle diameters, but rather inaccurate estimates of the PSD [5–7]. Also, these techniques exhibit increased sensitivity to the larger particles [5,6,8], and from this point of view they both seem adequate in principle for detecting and quantifying our contamination problem. In this work, the PSD is assumed to be bimodal, in order to avoid the ill-posed deconvolutions that are normally required for estimating a broad particle size distribution.

2. Theory

In single-angle DLS, a monochromatic laser light falls onto a dilute latex sample, with a photometer placed at a fixed angle θ_r with respect to the incident light. The photometer collects the light scattered over a small solid angle. The particle Brownian motions induce temporal fluctuations in the scattered light, and a devoted digital correlator calculates the (second-order) autocorrelation of the light intensity. We shall here indicate this function with $G^{(2)}_{\theta_r}(\tau_j)$, where τ_j (with $j = 1, \ldots, M_{\mathrm{DLS}}$) is the discrete time lag. From the autocorrelation, the PSD and/or the DLS average diameter ($\bar{D}_{\mathrm{DLS}}$) can be independently calculated [8,9]. In MDLS, the autocorrelations at all measuring angles are stored and processed, with certain advantages over single-angle DLS [10].

T measurements are normally carried out on UV–vis spectrophotometers. The turbidity spectrum represents the loss of intensity (at 180°) of the incident beam after passing through a dilute latex sample vs the incident wavelength λ_j. The spectrum is represented by $T(\lambda_j) = \log[I_0(\lambda_j)/I(\lambda_j)]$, where I_0 and I are the incident and emerging beam intensities, respectively [5,6], and ($j = 1, \ldots, M_{\mathrm{T}}$). Ideally, the turbidity should only be a measure of the scattered light; and this implies that light absorption is expected to be negligible [5,6,11].

We shall indicate a discrete number PSD by $f(D_i)$, where f is the number of particles contained in the diameter interval $[D_i, D_{i+1}]$. The $i = 1, 2, \ldots, N$ nonzero points of $f(D_i)$ are evenly spaced along the interval $[D_{\min}, D_{\max}]$. Thus, $D_i = D_{\min} + (i-1)\Delta D$, with $\Delta D = (D_{\max} - D_{\min})/(N-1)$. If $f(D_i)$ is known, then the following average diameters can be calculated:

$$\bar{D}_{a,b} = \left[\frac{\sum_{i=1}^{N} f(D_i) D_i^a}{\sum_{i=1}^{N} f(D_i) D_i^b}\right]^{1/(a-b)}, \quad a, b = 1, 2, 3, \ldots, \quad a > b. \tag{1}$$

In particular, $\bar{D}_{1,0}$ is the number-average diameter $\bar{D}_{\mathrm{n}}$, and $\bar{D}_{4,3}$ is the weight-average diameter $\bar{D}_{\mathrm{w}}$.

In single-angle DLS, the following must be inverted to estimate $f(D_i)$ [10],

$$g^{(1)}_{\theta_r}(\tau_j) = k_{\theta_r} \sum_{i=1}^{N} e^{-\Gamma_0(\theta_r)\tau_j/D_i} C_{I,\theta_r}(D_i) f(D_i), \quad \theta_r = \theta_1, \theta_2, \ldots, \theta_R, \quad j = 1, \ldots, M_{\mathrm{DLS}} \tag{2a}$$

with

$$G^{(2)}_{\theta_r}(\tau_j) = G^{(2)}_{\infty,\theta_r}\left\{1 + \beta\left|g^{(1)}_{\theta_r}(\tau_j)\right|^2\right\}, \quad \theta_r = \theta_1, \theta_2, \ldots, \theta_R, \quad j = 1, \ldots, M_{\mathrm{DLS}}, \tag{2b}$$

$$\Gamma_0(\theta_r) = \frac{16}{3}\pi\left(\frac{n_{\mathrm{m}}}{\lambda_{\mathrm{DLS}}}\right)^2 \frac{kT_0}{\eta} \sin^2\left(\frac{\theta_r}{2}\right), \quad \theta_r = \theta_1, \theta_2, \ldots, \theta_R, \tag{2c}$$

where $g^{(1)}_{\theta_r}(\tau_j)$ is the first-order autocorrelation of the electric field, as obtained from Eq. (2b); k_{θ_r} is a constant (for a given θ_r); the function $C_{I,\theta_r}(D_i)$ is given by the Mie theory [12,13], and represents the fraction of light intensity scattered at θ_r by a spherical particle of diameter D_i (for fixed values of the light polarization, the laser wavelength, and the refractive indices of the particles and the medium) [12,13]; $G^{(2)}_{\infty,\theta_r}$ is the autocorrelation baseline; β (<1) is an "instrumental" constant; λ_{DLS} is the in vacuo wavelength of the incident laser light; n_{m} is the refractive index of the (nonabsorbing) medium at λ_{DLS}; k is the Boltzmann constant; T_0 is the absolute temperature; and η is the

medium viscosity. In MDLS, Eqs. (2) are applied at R detection angles, and an optimization problem must be solved to calculate the best global PSD estimate [10,14,15].

In single-angle DLS, an average diameter (represented by $\bar{D}_{\mathrm{DLS}}$) can be calculated through the cumulants method [16] from the autocorrelation and knowledge of T_0, η, and n_{m}. The reproducibility of the DLS average diameter is around ±1%.

In T, the following expression must be inverted to calculate $f(D_i)$ [5,6],

$$T(\lambda_j) = \sum_{i=1}^{N} Q_{\mathrm{ext}}\big[D_i, \lambda_j, m_j(\lambda_j)\big] D_i^2 f(D_i),$$
$$m_j(\lambda_j) = n_{\mathrm{p}}(\lambda_j)/n_{\mathrm{m}}(\lambda_j), \quad j = 1, \ldots, M_{\mathrm{T}}, \tag{3}$$

where $T(\lambda_j)$ is the turbidity spectrum; $Q_{\mathrm{ext}}[D_i, \lambda_j, m_j(\lambda_j)]$ is the particle extinction efficiency (also obtained from the Mie theory); $m_j(\lambda_j)$ is the relative refractive index function; and $n_{\mathrm{p}}(\lambda_j)$, $n_{\mathrm{m}}(\lambda_j)$ are the refractive index functions for the particles and the medium, respectively [12,13]. Note that while the relative refractive index function is necessary for solving Eq. (3), MDLS only requires the refractive indexes of polymer and medium at the fixed measurement wavelength.

If the PSD is assumed uniform, then a T-average particle diameter $\bar{D}_{\mathrm{T}}$ can be calculated from

$$\bar{D}_{\mathrm{T}}(\lambda_j) = \frac{3c}{2\rho T(\lambda_j)} Q_{\mathrm{ext}}\big[\bar{D}_{\mathrm{T}}, \lambda_j, m_j(\lambda_j)\big], \tag{4}$$

where c is the polymer mass concentration; ρ is the polymer density; and $Q_{\mathrm{ext}}[\bar{D}_{\mathrm{T}}, \lambda_j, m_j(\lambda_j)]$ is obtained from the Mie theory. For accurate measurements of $\bar{D}_{\mathrm{T}}(\lambda_j)$, reasonably accurate values of the c/ρ ratio and of the relative refractive index function $m_j(\lambda_j)$, are required. Furthermore, since $Q_{\mathrm{ext}}[\bar{D}_{\mathrm{T}}, \lambda_j, m_j(\lambda_j)]$ is itself a function of the average diameter, an iterative procedure is necessary for calculating $\bar{D}_{\mathrm{T}}(\lambda_j)$. The oscillatory nature of $Q_{\mathrm{ext}}[\bar{D}_{\mathrm{T}}, \lambda_j, m_j(\lambda_j)]$ determines that multiple solutions can be obtained through Eq. (4); and to avoid this problem it is necessary to constraint the feasible range of $\bar{D}_{\mathrm{T}}(\lambda_j)$.

When the PSD is estimated by direct inversion of Eqs. (2) or (3), large errors are produced due to the ill-conditioned nature of the deconvolution operations. In contrast, the estimates of the ($\bar{D}_{\mathrm{DLS}}$ and $\bar{D}_{\mathrm{T}}$) average diameters are normally fast and accurate. Unfortunately, however, these averages are both a function of the measuring conditions: $\bar{D}_{\mathrm{DLS}}$ depends on the detection angle θ_r, and $\bar{D}_{\mathrm{T}}$ depends on the incident wavelength λ_j. Furthermore, neither $\bar{D}_{\mathrm{DLS}}$ nor $\bar{D}_{\mathrm{T}}$ can be associated with any absolute $\bar{D}_{a,b}$ average, except in the following (rather specific) situations. When the PSD is inside the so-called Rayleigh region (e.g., all particles are smaller than 50 nm), then (a) C_{I,θ_r} becomes proportional to D^6 and therefore $\bar{D}_{\mathrm{DLS}}$ tends toward $\bar{D}_{6,5}$, and (b) Q_{ext} becomes proportional to D^4 and therefore $\bar{D}_{\mathrm{T}}$ tends toward $\bar{D}_{6,3}$. In contrast, at the limit of the very large particles, $\bar{D}_{\mathrm{T}}$ tends toward $\bar{D}_{3,2}$ and $Q_{\mathrm{ext}} \cong 2$ [5,6].

Finally, if the PSD is known, then theoretical estimates of the average diameters can be obtained from [6,10],

$$\bar{D}_{\mathrm{DLS}}(\theta_r) = \frac{\sum_{i=1}^{N} f(D_i) C_{I,\theta_r}(D_i)}{\sum_{i=1}^{N} f(D_i) C_{I,\theta_r}(D_i)/D_i} \tag{5}$$

and

$$\bar{D}_{\mathrm{T}}(\lambda_j) = Q_{\mathrm{ext}}\big(\bar{D}_{\mathrm{T}}, \lambda_j, m_j\big) \times \frac{\sum_{i=1}^{N} D_i^3 f(D_i)}{\sum_{i=1}^{N} D_i^2 Q_{\mathrm{ext}}(D_i, \lambda_j, m_j) f(D_i)}. \tag{6}$$

2.1. Proposed data treatment

In what follows, assume that the main population diameter D_1 is known and that the PSD is bimodal. The contamination is characterized by unknown values of D_2 ($D_2 > D_1$) and $f_2 = 1 - f_1$ ($f_2 \ll f_1$), and our aim is to find the pair (D_2, f_2).

The following iterative procedures were applied to MDLS measurements only, T measurements only, and combined MDLS–T: (i) guess an initial pair (D_2, f_2); (ii) from the resulting bimodal PSD, predict either the raw measurements (through Eqs. (2) or (3)), or some average diameter (through Eqs. (5) or (6)); (iii) evaluate a functional involving an average squared error between a measurement and the predicted measurement (or between a "measured" average diameter and the predicted average diameter); and (iv) iterate until (D_2, f_2) is found that minimizes the sought functional. Consider now some (from the many possible) minimization functionals.

For MDLS measurements only, one can either estimate the complete set of measurements $G^{(2)}_{\theta_r,\mathrm{exp}}(\tau_j)$, or their derived $\bar{D}_{\mathrm{DLS,exp}}(\theta_r)$. The following functionals are proposed,

$$J_{G^{(2)}} = \frac{1}{R} \sum_{r=1}^{R} \frac{1}{M_{\mathrm{DLS}}} \left\{ \sum_{j=1}^{M_{\mathrm{DLS}}} \left[1 - \frac{\hat{G}^{(2)}_{\theta_r}(\tau_j)}{G^{(2)}_{\theta_r,\mathrm{exp}}(\tau_j)} \right]^2 \right\}^{1/2} \tag{7}$$

and

$$J_{\bar{D}_{\mathrm{DLS}}} = \frac{1}{R} \left\{ \sum_{r=1}^{R} \left[1 - \frac{\hat{\bar{D}}_{\mathrm{DLS}}(\theta_r)}{\bar{D}_{\mathrm{DLS,exp}}(\theta_r)} \right]^2 \right\}^{1/2}, \tag{8}$$

where R and M_{DLS} are the number of detection angles and of autocorrelation points, respectively, and $\hat{G}^{(2)}_{\theta_r}(\tau_j)$ and $\hat{\bar{D}}_{\mathrm{DLS}}(\theta_r)$ are the estimated autocorrelations and average diameters, calculated by introducing the bimodal PSD (given by (D_1, $1 - f_2$) and (D_2, f_2)) into Eqs. (2) and (5), respectively.

Equation (8) is considerably simpler than Eq. (7). Also, the optimizations involved the adjustment of only two parameters (D_2 and f_2); and to this effect, $\bar{D}_{\mathrm{DLS}}(\theta_r)$ was seen to contain enough information for their reasonable estimation. Even though Eq. (8) was preferably selected, Eq. (7) was also tested for Latex 2.

For T measurements only, one can either estimate the raw spectrum $T(\lambda_j)$, or its derived function $D_{\mathrm{T}}(\lambda_j)$. The following functionals are here proposed,

$$J_T = \frac{1}{M_{\mathrm{T}}}\left\{\sum_{j=1}^{M_{\mathrm{T}}}\left[1-\frac{\hat{T}(\lambda_j)}{T_{\exp}(\lambda_j)}\right]^2\right\}^{1/2} \tag{9}$$

and

$$J_{\bar{D}_{\mathrm{T}}} = \frac{1}{M_{\mathrm{T}}}\left\{\sum_{j=1}^{M_{\mathrm{T}}}\left[1-\frac{\hat{\bar{D}}_{\mathrm{T}}(\lambda_j)}{\bar{D}_{\mathrm{T,exp}}(\lambda_j)}\right]^2\right\}^{1/2}, \tag{10}$$

where M_{T} is the number of points of the turbidity spectrum and $\hat{T}(\lambda_j)$ and $\hat{\bar{D}}_{\mathrm{T}}(\lambda_j)$ are estimates of the measured spectrum and average diameter function, obtained by introducing $(D_1, 1-f_2)$ and (D_2, f_2) into Eqs. (3) and (6), respectively. Since $\bar{D}_{\mathrm{T}}(\lambda_j)$ in Eq. (10) may involve multiple solutions, then Eq. (9) was the selected functional for processing the T measurements.

For combined MDLS–T measurements, the following mixed functional is proposed:

$$J_{\mathrm{MDLS-T}} = \omega\frac{J_{\bar{D}_{\mathrm{DLS}}}}{J_{\bar{D}_{\mathrm{DLS}_{\min}}}} + (1-\omega)\frac{J_T}{J_{T_{\min}}} \tag{11}$$

where ω ($\leqslant 1$) is an adjustable weighting factor and $J_{\bar{D}_{\mathrm{DLS}_{\min}}}$ and $J_{T_{\min}}$ are the solutions minimizing Eqs. (8) and (9), respectively. For $\omega = 1$, the solution for [min $J_{\mathrm{MDLS-T}}$] is expected to coincide with that of $J_{\bar{D}_{\mathrm{DLS}_{\min}}}$, and [min $J_{\mathrm{MDLS-T}}$] $\cong 1$. For $\omega = 0$, the solution for [min $J_{\mathrm{MDLS-T}}$] is expected to coincide with that of $J_{T_{\min}}$, and again [min $J_{\mathrm{MDLS-T}}$] $\cong 1$. Each term on the r.h.s. of Eq. (11) is normalized with the final values of $J_{\bar{D}_{\mathrm{DLS}}}$ and J_T. The reason is to compensate for possible large differences between the numerical values of $J_{\bar{D}_{\mathrm{DLS}_{\min}}}$ and $J_{T_{\min}}$, which could introduce bias into the combined solution.

3. Experimental work

The latex that was synthesized in our laboratories (Latex 1) was analyzed by SEM, MDLS, and T. The latex that was obtained by simple blending of standards (Latex 2) was analyzed by MDLS and T. In these last two analyses, the measuring conditions and data treatment procedures coincided with those of Latex 1.

3.1. Analysis of Latex 1

The SEM equipment was a JEOL-JSM 35C. For the sample preparation, the latex was diluted, a droplet was dried on a glass sample holder, and a Veeco evaporator was used for covering the particles with a film of gold. The microscope was calibrated with a PS standard latex from Polyscience, of nominal diameter 1.1 μm. Fig. 1 shows two micrographs of our synthesized latex. Most micrographs only exhibited

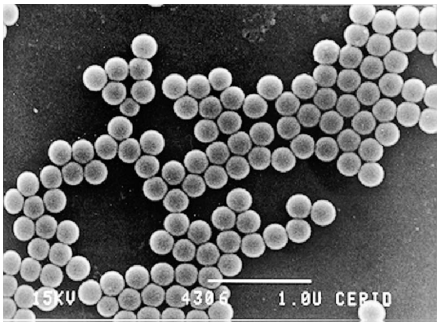

(a)

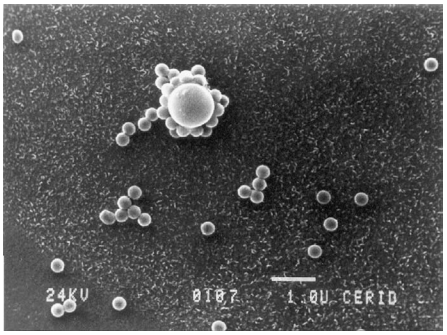

(b)

Fig. 1. SEM micrographs of Latex 1 (our synthesized PS latex) showing (a) the main population of particles and (b) a large contaminating particle immersed in the main population.

the main population of particles (Fig. 1a). But some micrographs also exhibited much larger particles, around 950 nm (Fig. 1b). After counting 500 particles of the main population, its number-average diameter resulted 340 nm.

The DLS instrument was a laser light-scattering photometer from Brookhaven Instruments Inc., fit with a vertically polarized He–Ne laser at 632.8 nm, and a digital correlator (Model BI-2000 AT). The measurements were carried out at 25 °C, and at the following detection angles: 30°, 40°, 50°, 60°, 70°, 80°, 90°, 100°, 110°, 120°, 130°, and 140°. To avoid multiple scattering, the latex concentration was adjusted at each detection angle, to yield around 200,000 counts/s, along measuring times ranging between 100 and 200 s [10]. Fig. 2a presents the normalized measured autocorrelations in the format $(G^{(2)}_{\theta_r}(\tau_j) - G^{(2)}_{\infty,\theta_r})/(G^{(2)}_{\theta_r}(0) - G^{(2)}_{\infty,\theta_r})$. The slopes of the autocorrelations taken at 120°, 130°, and 140°(in the dashed trace) are lower than the curves at smaller angles.

The turbidity spectrum was obtained with a UV–vis spectrophotometer from Perkin–Elmer (Lambda 20 model). To avoid multiple scattering, the latex was diluted to 3×10^{-5} g/cm^3. The spectrum contains 551 points at 1-nm intervals in the range 350–900 nm (Fig. 3a). Light absorption is almost negligible at the given conditions.

The DLS average diameter was calculated through the quadratic cumulants method [16] from the set of autocorrelations and the following constants: $k = 0.0138$ g nm^2/s^2 K; $\lambda_{\mathrm{DLS}} = 632.8$ nm; $n_{\mathrm{m}} = 1.3316$; $T_0 = 298.15$ K; and $\eta = 0.89 \times 10^{-9}$ g/nm s. The resulting average diameter is

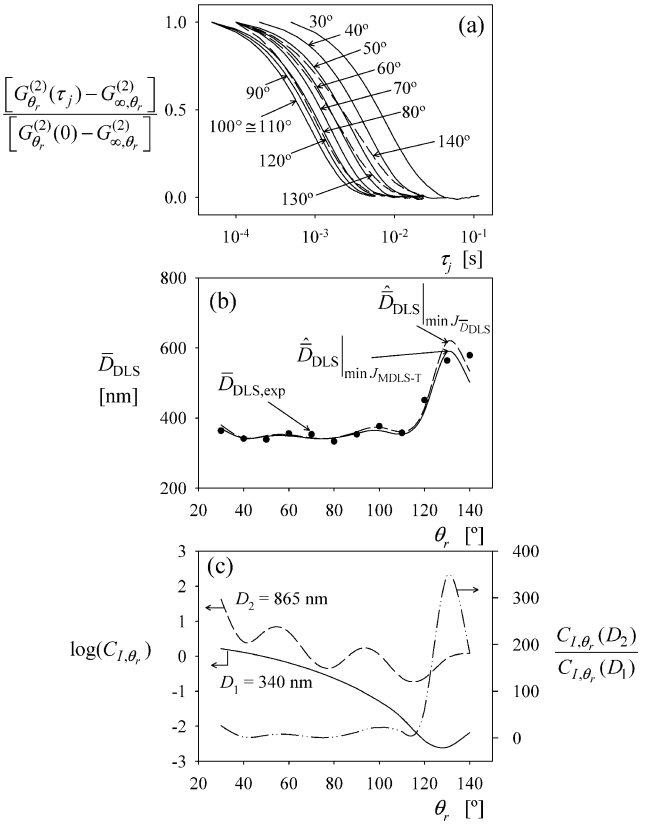

Fig. 2. MDLS measurements of Latex 1 (our synthesized PS latex). (a) Normalized autocorrelation functions at the measured detection angles. (b) DLS average diameter as a function of the detection angle. (c) Mie functions and their ratio, for $D_1 = 340$ nm (the TEM value) and for $D_2 = 865$ nm (as estimated by MDLS–T). The experimental average diameters are represented with dots; while their theoretical predictions were obtained by injecting into Eq. (5) the bimodal PSDs estimated by MDLS only and MDLS–T.

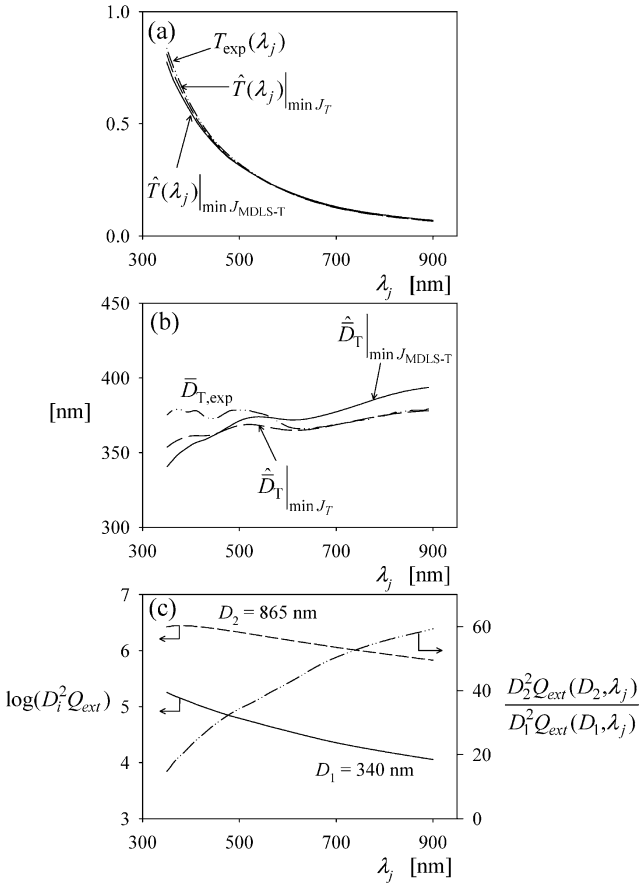

Fig. 3. T measurements of Latex 1 (our synthesized PS latex). (a) Experimental turbidity spectrum and two of its theoretical predictions calculated from the bimodal PSD estimates obtained by T only and MDLS–T. (b) T average diameters as a function of the wavelength. (c) "Turbidimetric" Mie functions and their ratio for $D_1 = 340$ nm (the TEM value) and for $D_2 = 865$ nm (as estimated by MDLS–T). The direct experimental measurements are compared with their theoretical predictions calculated from the bimodal PSD estimates obtained by T only and MDLS–T.

represented by dots in Fig. 2b. As we shall see later, the initial (rather moderate) oscillations of $\bar{D}_{\mathrm{DLS,exp}}(\theta_r)$, together with its final increase for angles greater than 110°, is indicative of a contamination by larger particles.

The T average diameters were calculated through Eq. (4), from the turbidity spectrum and the following set of data: $c = 3 \times 10^{-5}$ g/cm^3; $\rho = 1.04$ g/cm^3; $n_{\mathrm{m}}(\lambda_j)$ for pure water, as in Ref. [17]; and $n_{\mathrm{p}}(\lambda_j)$ for PS, as in Ref. [18]. The resulting $\bar{D}_{\mathrm{T,exp}}(\lambda_j)$ is presented in Fig. 3b. After some initial oscillations, this function grows monotonically for $\lambda_j > 600$ nm; thus indicating that $\bar{D}_{\mathrm{T,exp}}$ exhibits an increased sensitivity to the larger particles at the larger wavelengths.

3.2. Analysis of Latex 2

Latex 2 was especially prepared to emulate our synthesized latex, but with a (nominally) strictly bimodal distribution. It was obtained by simple blend of two PS standards from Polyscience, of nominal diameters $D_1 = 306$ nm and $D_2 = 974$ nm. The number fraction of the larger-sized particles was gravimetrically determined, yielding $f_2 \approx 2\%$ (and therefore $f_1 \approx 98\%$). For this determination, only small amounts of latex were used, thus explaining the "approximately equal" signs. Also, it was assumed that the density of the polymer particles in the latex coincided with the density of the dry polymer.

The raw measurements and average diameters are presented in Figs. 4a, 5a and 4b, 5b, respectively. $\bar{D}_{\mathrm{DLS,exp}}(\theta_r)$ is oscillatory for angles up to 90°, and then it increases monotonically (Fig. 4b). In contrast, $\bar{D}_{\mathrm{T,exp}}(\lambda_j)$ increases monotonically with the wavelength (Fig. 5b).

The errors in the estimated diameters are the consequence of the following: (i) systematic measurement errors, intrinsic to the instrumental hardware and software; and (ii) uncertainties in the variables that are required in the data treatment, such as the relative refractive index function and the mass density. The deviations are difficult to quantify, and a detailed propagation of errors study would be required. Fig. 5b illustrates the effect of introducing a 10% error in the polymer concentration c, while maintaining all other variables unchanged. In this case, $\bar{D}_{\mathrm{T,exp}}(\lambda_j)$ is underestimated by around 10%.

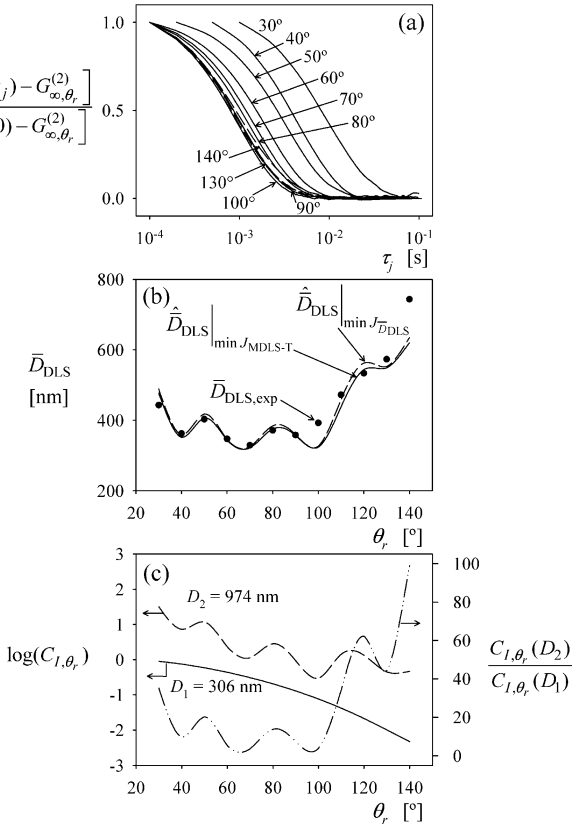

Fig. 4. MDLS measurements of Latex 2 (a bimodal PSD with ($f_1 \approx 98\%$, $D_1 = 306$ nm) and ($f_2 \approx 2\%$, $D_2 = 974$ nm), obtained by mixing two PS standards). (a) Normalized autocorrelations at the measured detection angles. (b) DLS average diameters as a function of the detection angle. (c) Mie functions and their ratio for the nominal diameters: $D_1 = 306$ nm and $D_2 = 974$ nm. The experimental average diameters (represented by dots) are compared with their theoretical predictions obtained from the bimodal PSDs estimated by MDLS only and by combined MDLS–T.

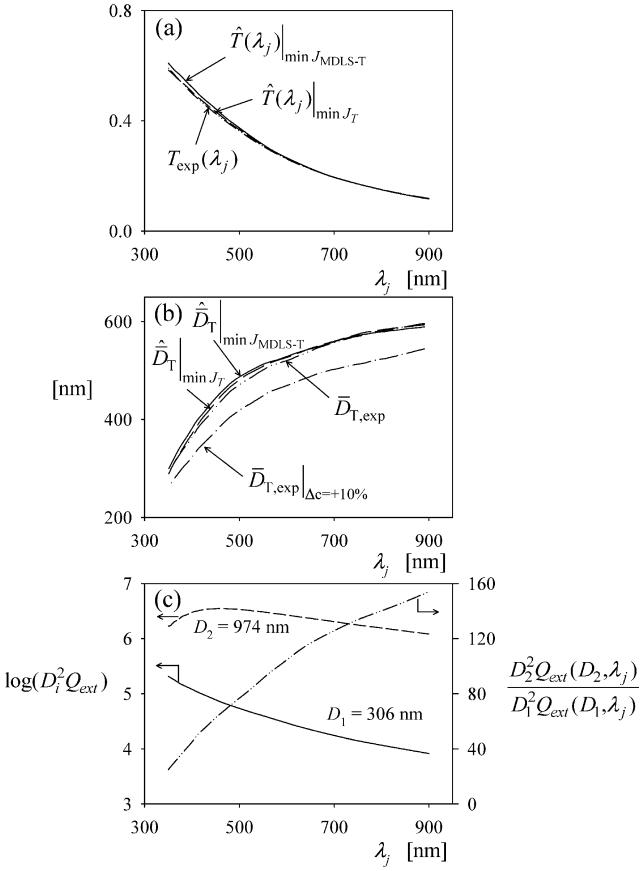

Fig. 5. T measurements of Latex 2 (a bimodal PSD with ($f_1 \approx 98\%$, $D_1 = 306$ nm) and ($f_2 \approx 2\%$, $D_2 = 974$ nm), obtained by mixture of PS standards). (a) Experimental turbidity spectrum and two of its predictions obtained from bimodal PSDs estimated by T only and by MDLS–T. (b) T average diameters as a function of the wavelength. (c) "Turbidimetric" Mie functions and their ratio, for the nominal diameters $D_1 = 306$ nm and $D_2 = 974$ nm. The direct measurements are compared with theoretical predictions obtained by T only and by MDLS–T. Also shown is the effect on the average diameter of a 10% error in the polymer mass concentration.

Table 1
Contamination of Latex 2 (a mixture of two PS standards with ($D_1 = 306$ nm, $f_1 \approx 98\%$), and ($D_2 = 974$ nm, $f_2 \approx 2\%$)), as determined by the three investigated data treatment procedures

Data treatment	$\hat{D}_2$ (nm)	$\hat{f}_2$	Minimized functional	Final functional value
MDLS only	963	0.032	$J_{\bar{D}_{\mathrm{DLS}}}$ [a]	0.02187
MDLS only	968	0.035	$J_{G^{(2)}}$ [b]	0.00060
T only	994	0.025	J_T [c]	0.00085
MDLS–T	967	0.028	$J_{\mathrm{MDLS-T}}$ [d]	1.11

[a] Equation (8).
[b] Equation (7).
[c] Equation (9).
[d] Equation (11) with $\omega = 0.5$.

4. Results and discussion

First, the MDLS only and T only problems were solved through Eqs. (8) and (9), respectively. Then, the mixed functional of Eq. (11) was minimized, adopting $\omega = 0.5$. This value implies that each individual set of measurements is equally weighed. In all the minimizations, the search was bounded as follows: $D_1 < D_2 < 1500$ nm (at intervals of 1 nm); and $0 < f_2 < 0.05$ (at intervals of 0.001). Some correlation between the estimates of D_2 and f_2 might be expected. Fortunately however, global minima were found in all cases, without reaching the bounds for D_2 or f_2. Consider first the results for Latex 2 (i.e., the sample containing the best a priori known PSD).

4.1. Data treatment for Latex 2

In this case, the bimodality requirement was strictly verified, and the PSD was nominally given by ($D_1 = 306$ nm, $f_1 \approx 98\%$) and ($D_2 = 974$ nm, $f_2 \approx 2\%$). For the data treatment, $D_1 = 306$ nm was adopted. The final results are presented in Table 1. For the MDLS-only case, solutions were found that involved $J_{\bar{D}_{\mathrm{DLS}}}$ of Eq. (8) and $J_{G^{(2)}}$ of Eq. (7). In both cases, similar results are observed: while D_2 appears underestimated with respect to the nominal value, f_2 results are overestimated. The final value of $J_{G^{(2)}}$ is considerably lower than that of $J_{\bar{D}_{\mathrm{DLS}}}$. However, these numerical values

Table 2
Contamination of Latex 1 (our synthesized PS latex), as determined by the three investigated data treatment procedures

Data treatment	$\hat{D}_2$ (nm)	$\hat{f}_2$	Minimized functional	Final functional value
MDLS only	867	0.008	$J_{\bar{D}_{\mathrm{DLS}}}$ [a]	0.01276
T only	614	0.022	J_T [b]	0.00077
MDLS–T	865	0.006	$J_{\mathrm{MDLS-T}}$ [c]	1.80

[a] Equation (8).
[b] Equation (9).
[c] Equation (11) with $\omega = 0.5$.

Table 3
Average diameters of three proposed bimodal PSDs (with $D_1 = 300$ nm and $D_2 = 900$ nm)

f_2	$\bar{D}_{\mathrm{n}}$	$\bar{D}_{\mathrm{w}}$
0.02	312.0	513.2
0.06	336.0	679.7
0.10	360.0	750.0

do not provide any indication of the quality of the results, due to the very large difference in the numerical values of the involved calculation variables.

The last two rows of Table 1 present the solutions for the T-only case and the combined MDLS–T case. While the minimization of J_T yielded the best prediction for f_2 ($= 2.5\%$), the minimization of $J_{\mathrm{MDLS-T}}$ produced a good prediction for D_2 ($= 967$ nm). Again, the final functional values provide little additional information, and their comparison is not useful. Also, the large differences in the numerical values of $J_{T_{\min}}$ and $J_{\bar{D}_{\mathrm{DLS}_{\min}}}$ justifies the normalizations in Eq. (11).

Fig. 4b exhibits the predicted evolutions of $\bar{D}_{\mathrm{DLS}}(\theta_r)$ for the MDLS only and the combined MDLS–T cases, obtained by introducing the resulting bimodal PSDs into Eq. (5). The fit is excellent at the lower observation angles, but relatively large differences are seen at the observation angles 100° and 140°. To help interpret these results, Fig. 4c shows the Mie functions $C_{I,\theta_r}(D_i)$ for the a priori known nominal diameters, together with their ratio $C_{I,\theta_r}(D_2)/C_{I,\theta_r}(D_1)$. Note that (except for a constant), the oscillations in the estimated $\bar{D}_{\mathrm{DLS}}(\theta_r)$ are proportional to the Mie ratio. This rather interesting conclusion can be directly derived from Eq. (5).

Fig. 5a exhibits the predicted turbidity spectra for the T-only and combined MDLS–T cases, as obtained by introducing their resulting bimodal PSDs into Eq. (3). In general, the fits are good, and the largest deviations are observed at the lowest wavelengths. Fig. 5c shows the products $D_1^2 Q_{\mathrm{ext}}(D_1, \lambda_j)$ and $D_2^2 Q_{\mathrm{ext}}(D_2, \lambda_j)$ for (the a priori known diameters) $D_1 = 306$ nm and $D_2 = 974$ nm, together with the "turbidimetric" Mie ratio $D_2^2 Q_{\mathrm{ext}}(D_2, \lambda_j)/D_1^2 Q_{\mathrm{ext}}(D_1, \lambda_j)$. From Eq. (6), it can be proven that $\bar{D}_{\mathrm{T}}(\lambda_j)$ is mainly a function of this last ratio. Both $\bar{D}_{\mathrm{T}}(\lambda_j)$ and the Mie ratio increase monotonically with λ_j, and this determines the greater sensitivity of $\bar{D}_{\mathrm{T}}(\lambda_j)$ to the larger particles at the higher wavelengths.

The deviations in the contamination estimates are a consequence of (a) errors in the raw functions (i.e., $\bar{D}_{\mathrm{DLS}}(\theta_r)$ and the turbidity spectrum) and (b) errors introduced by the optimization procedure. Compared with the nominal values, the combined MDLS–T exhibits a 1% error in D_2, and a 40% error in f_2. This last (rather large) difference may be more due to errors in the nominal f_2 value obtained by gravimetry, than on errors via the optimization technique. Furthermore, the employed standards could themselves include some contamination by larger particles.

4.2. Data treatment for Latex 1

Here, we adopted $D_1 = 340$ nm, as measured by SEM. The results of minimizing $J_{\bar{D}_{\mathrm{DLS}}}$, J_T, and $J_{\mathrm{MDLS-T}}$ are presented in Table 2. Compared with the previous case, larger differences are seen between the estimates by MDLS only and by T only. The MDLS–T results are close to the MDLS only estimates. Also, the MDLS results are not intermediate between the individual estimates by MDLS only and T only. This loss of consistency may be due to the fact that the large particles of Latex 1 are not strictly unimodal. The contamination diameters by MDLS only and by MDLS–T (867 and 865 nm, respectively) are close to the SEM observations (Fig. 1b).

Fig. 2b represents the predictions for $\bar{D}_{\mathrm{DLS}}(\theta_r)$, obtained by MDLS only and by combined MDLS–T, when introducing their resulting bimodal PSDs into Eq. (5). Quite reasonable fits are observed. Fig. 2c exhibits the Mie functions $C_{I,\theta_r}(D_i)$ for $D_1 = 340$ nm and for the estimated $D_2 = 865$ nm, together with the Mie ratio $C_{I,\theta_r}(D_2)/C_{I,\theta_r}(D_1)$. As mentioned before, the oscillations in $\bar{D}_{\mathrm{DLS}}(\theta_r)$ are a consequence of the oscillatory Mie ratio.

Fig. 3a illustrates the predicted turbidity spectra for the T-only and the combined MDLS–T. The fits are excellent at the higher wavelengths, but diverge at the lower wavelengths. Fig. 3b compares the direct measurement of $\bar{D}_{\mathrm{T}}(\lambda_j)$ with its corresponding predictions by T only and MDLS–T, obtained by introducing their PSD estimates into Eq. (6). The predictions by T only are excellent at the higher wavelengths, but diverge at the lower wavelengths. The $\bar{D}_{\mathrm{T}}(\lambda_j)$ predictions by MDLS–T are not as good, possibly due to the large differences between the PSD estimates by MDLS–T and by T only. In Fig. 3c, the products $D_1^2 Q_{\mathrm{ext}}(D_1, \lambda_j)$ and $D_2^2 Q_{\mathrm{ext}}(D_2, \lambda_j)$ are represented vs λ_j for $D_1 = 340$ nm (the TEM value) and for $D_2 = 865$ nm (the MDLS–T result); together with the Mie ratio $D_2^2 Q_{\mathrm{ext}}(D_2, \lambda_j)/D_1^2 Q_{\mathrm{ext}}(D_1, \lambda_j)$. Even though this ratio increases monotonically, this is not the case of $\bar{D}_{\mathrm{T}}(\lambda_j)$, possibly due to the fact that Latex 1 is not strictly bimodal. In contrast, note that for the strictly bimodal Latex 2, both $\bar{D}_{\mathrm{T}}(\lambda_j)$ and $D_2^2 Q_{\mathrm{ext}}(D_2, \lambda_j)/D_1^2 Q_{\mathrm{ext}}(D_1, \lambda_j)$ increase monotonically with λ_j (Figs. 5b and 5c, respectively).

4.3. Final simulation results

Finally, let us theoretically investigate the sensitivity of $\bar{D}_{\mathrm{DLS}}(\theta_r)$ and $\bar{D}_{\mathrm{T}}(\lambda_j)$ to increasing amounts of larger particles. To this effect, three bimodal PSDs were defined, exhibiting identical diameters ($D_1 = 300$ nm and $D_2 = 900$ nm), but different amounts of the (larger) contaminating particles ($f_2 = 2$, 6, and 10%). For $f_2 = 0\%$, the system is strictly uniform at D_1. For $f_2 = 2\%$, the PSD is similar to our experimental samples. The absolute average diameters of the three distributions are given in Table 3, and the simulated evolutions for $\bar{D}_{\mathrm{DLS}}(\theta_r)$ and $\bar{D}_{\mathrm{T}}(\lambda_j)$ are presented in Figs. 6a and 6b, respectively. For $f_2 = 0$, all averages coincide at $D_1 = 300$ nm. For the three bimodal distributions, all the values of $\bar{D}_{\mathrm{DLS}}$ or $\bar{D}_{\mathrm{T}}$ fall within the expected range of 300–900 nm. Figs. 6a and 6b show that the largest sensitivities of $\bar{D}_{\mathrm{DLS}}$ and $\bar{D}_{\mathrm{T}}$ to the larger particles occur as f_2 tends to zero. Also, $\bar{D}_{\mathrm{DLS}}$ oscillates with θ_r, and its amplitude increases with f_2 (Fig. 6a). In contrast, $\bar{D}_{\mathrm{T}}$ increases monotonically with λ_j, but it flattens at the higher wavelengths (Fig. 6b). This last observation implies that if the spectrum only included the higher wavelengths, then it could be erroneously interpreted as belonging to a uniform PSD of some intermediate particle diameter.

In Fig. 6a, the larger deviations of $\bar{D}_{\mathrm{DLS}}$ with respect to the main population occur at the higher measurement angles. This is not generally so, however. Other simulation results (not presented here for reasons of space) have shown that for a bimodal PSD of diameters 100 and 300 nm, the highest sensitivities of $\bar{D}_{\mathrm{DLS}}$ were given at the lower observation angles. Similarly, for a bimodal PSD of diameters 400 and 1200 nm, the highest sensitivities of $\bar{D}_{\mathrm{DLS}}$ appear at the intermediate angles. In contrast, and irrespective of the PSD, the highest sensitivity of $\bar{D}_{\mathrm{T}}$ was always seen at the higher wavelengths. Unfortunately however, the turbidity spectrum exhibits a relatively low signal-to-noise ratio at the higher wavelengths.

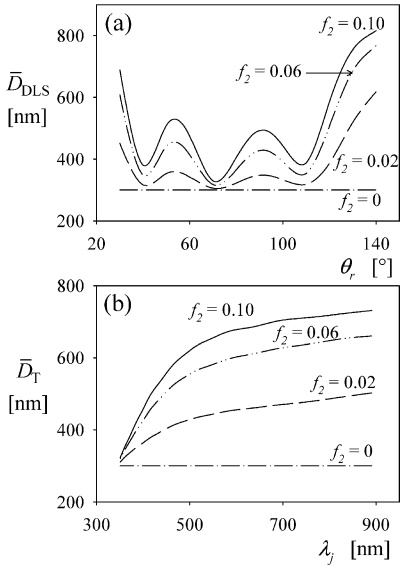

Fig. 6. Simulated predictions for three bimodal PSDs exhibiting $D_1 = 300$ nm and $D_2 = 900$ nm, but different number fractions of larger particles. (a) DLS average diameter as a function of the detection angle. (b) T average diameter as a function of the wavelength.

5. Conclusions

Often, "uniform" latices are contaminated by larger particles, and this contamination cannot be easily quantified by electron microscopy. The investigated optical techniques proved effective for quantifying a (small) contamination by larger particles, and their sensitivities were highest as the amount of contaminant tended to zero. In general, MDLS seems preferable to T, because the former technique requires of less a priori information for its data treatment. This could represent an important limitation for T when the nature of the particles and/or the medium is unknown, and therefore their optical parameters cannot be directly taken from the literature.

A data treatment procedure was proposed that is applicable to MDLS only, T only, or combined MDLS–T. It calculates the contamination of almost-uniform latices from the knowledge of the main population diameter and assuming a bimodal PSD. The procedure was applied onto two similar PS latices. For the latex obtained by mixture of two standards (Latex 2), the bimodality condition was strictly verified, and all the results were quite accurate. For the latex synthesized in our laboratory (Latex 1), relatively large differences between the estimates by MDLS only and T only were observed, and the combined MDLS–T did not provide intermediate results. In this case, the contamination diameters by MDLS only and by MDLS–T were close to the SEM observations. The inconsistencies in the results of Latex 1 are mainly due to the fact that the bimodality requirement was not strictly fulfilled, as verified from the shapes of the Mie ratio functions: $C_{I,\theta_r}(D_2)/C_{I,\theta_r}(D_1)$ vs θ_r and $D_2^2 Q_{\mathrm{ext}}(D_2, \lambda_j)/D_1^2 Q_{\mathrm{ext}}(D_1, \lambda_j)$ vs λ_j.

In the combined MDLS–T calculations, equal weights were chosen in Eq. (11) for the MDLS and T measurements. A better selection of the weighting factor in Eq. (11) would require introducing a priori information on the expected accuracy of the individual MDLS and T techniques.

Acknowledgment

We are grateful for the financial support received from CONICET, SeCyT, and the Universidad Nacional del Litoral (Argentina).

References

[1] T. Sugimoto, Monodispersed Particles, Academic Press, Amsterdam, 2001.
[2] C. Pichot, T. Delair, A. Elaïssari, in: J.M. Asua (Ed.), Polymeric Dispersions: Principles and Applications, in: NATO ASI Series, Se-

ries E: Applied Sciences, vol. 335, Kluwer Academic, Dordrecht, 1997, p. 515.
[3] J.M. Sáenz, J.M. Asua, J. Polym. Sci. Polym. Chem. A 33 (1995) 1511.
[4] V.D.G. Gonzalez, L.M. Gugliotta, J.R. Vega, G.R. Meira, in: Proceedings of Enpromer II, 2001, P. 847.
[5] T. Kourti, Ph.D. thesis, McMaster University, Canada, 1989.
[6] M.A. Llosent, L.M. Gugliotta, G.R. Meira, Rubber Chem. Technol. 69 (1996) 696.
[7] L.M. Gugliotta, J.R. Vega, G.R. Meira, J. Colloid Interface Sci. 228 (2000) 14.
[8] R. Pecora, Dynamic Light Scattering, Applications of Photon Correlation Spectroscopy, Plenum, New York, 1985.
[9] B. Chu, Laser Light Scattering, Academic Press, New York, 1991.
[10] J.R. Vega, L.M. Gugliotta, V.D.G. Gonzalez, G.R. Meira, J. Colloid Interface Sci. 261 (2003) 74.
[11] G. Eliçabe, L. García-Rubio, in: C. Craver, T. Provder (Eds.), Polymer Characterization. Physical Property, Spectroscopic, and Chromatographic Methods, in: Advances in Chemistry Series, vol. 227, American Chemical Society, Washington, DC, 1990, p. 83.
[12] G. Mie, Ann. Phys. 25 (1908) 337.
[13] C.F. Bohren, D.R. Huffman, Absorption and Scattering of Light by Small Particles, Wiley, New York, 1983.
[14] S.E. Bott, in: P.J. Lloyd (Ed.), Particle Size Analysis, Wiley, New York, 1988, p. 77.
[15] G. Bryant, C. Abeynayake, J. Thomas, Langmuir 12 (1996) 6224.
[16] D.E. Koppel, J. Chem. Phys. 57 (1972) 4814.
[17] M. Kerker, The Scattering of Light and Other Electro-Magnetic Radiation, Academic Press, New York, 1969.
[18] T. Inagaki, E.T. Arakawa, R.N. Hamm, M.W. Williams, Phys. Rev. B 15 (1977) 3243.